Supporting Information

A Supramolecular Strategy to Engineering a Non-Photobleaching and Near-Infrared Absorbing Nano-J-Aggregate for Efficient Photothermal Therapy

Meihui Su,[†,‡,#] Qiuju Han,[†,#] Xiaosa Yan,[†,‡] Yanan Liu,[†,‡] Pei Luo,[†,‡] Wenhao Zhai,[†,‡] Qiangzhe Zhang,[*,†] Luyuan Li,[†] and Changhua Li[*,†,‡]

[†]State Key Laboratory of Medicinal Chemical Biology, College of Pharmacy and Tianjin Key Laboratory of Molecular Drug Research, Nankai University, Tianjin 300071, China. [‡]Key Laboratory of Functional Polymer Materials of Ministry of Education, Nankai University, Tianjin 300071, China.

1. Materials and Instruments

1,3-diphenylisobenzofuran (DPBF) and indocyanine green (ICG) were purchased from Sigma-Aldrich. Amphiphilic copolymer poly(ethylene glycol)$_{113}$-*b*-poly(caprolactone)$_8$ (PEG-PCL)[1] and 4-(3-phenyltzobenzofuryl)phenyl trimethylammonium iodide (QDPBF)[2] were synthesized according to previous literature procedures. Dynamic light scattering (DLS) studies were performed using a Zetasizer NanoZS (Malvern). Morphological analyses were conducted on transmission electron microscopy (TEM; Talos F200C, FEI), atomic force microscopy (AFM; Dimension Icon, Bruker), and scanning electron microscopy (SEM; MERLIN Compact, ZEISS). UV-vis absorption spectra were recorded on a UH5300 double-beam UV-Vis spectrophotometer (Hitachi). Fluorescence emission spectra were recorded on a F4600 (Hitachi) spectrofluorometer. CCK-8 assay was monitored by the microplate reader (SpectraMax i3x, MD). Confocal laser scanning microscopy (CLSM) images were acquired using a Leica TCS SP8 microscope. The laser sources used are MRL-III-655R (λ_{em} = 655 nm), MRL-III-785 (λ_{em} = 785 nm), and MDL-H-808 (λ_{em} = 808 nm) semiconductor lasers (CNI, Changchun, China). The temperature changes induced by photothermal effect were recorded using an infrared thermal camera (FLIR E60).

2. Synthesis of BDP-H and BDP

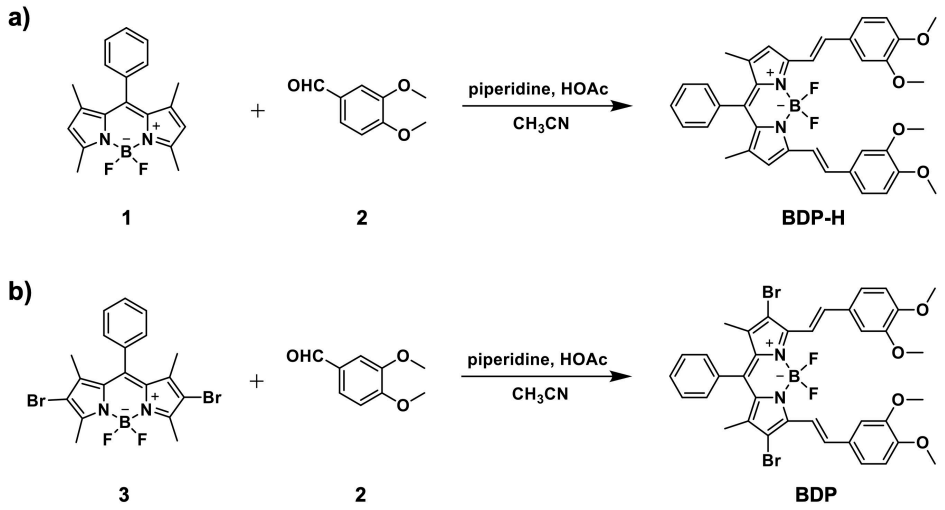

Scheme S1. Synthetic routes employed for the preparation of **BDP-H** (a) and **BDP** (b).

Compounds **BDP-H** and **BDP** were synthesized according to our previously reported procedures.[3] Data for **BDP-H:** ^{1}H NMR (400 MHz, $CDCl_3$, Figure S23) δ (ppm) 7.60 (d, J = 16.2 Hz, 2H), 7.50 (tq, J = 4.7, 2.6, 1.9 Hz, 3H), 7.39–7.31 (m, 2H), 7.24–7.17 (m, 4H), 7.15 (d, J = 2.0 Hz, 2H), 6.89 (d, J = 8.4 Hz, 2H), 6.62 (s, 2H), 3.96 (d, J = 19.0 Hz, 12H), 1.44 (s, 6H). Data for **BDP:** ^{1}H NMR (400 MHz, $CDCl_3$, Figure S24) δ (ppm) 8.08 (d, J = 16.5 Hz, 2H), 7.61 (d, J = 16.6 Hz,

2H), 7.54 (d, J = 4.7 Hz, 3H), 7.31 (d, J = 4.8 Hz, 2H), 7.24 (d, J = 8.3 Hz, 2H), 7.16 (s, 2H), 6.90 (d, J = 8.3 Hz, 2H), 3.96 (d, J = 13.0 Hz, 12H), 1.42 (s, 6H).

3. Characterization and Properties of J-NS and J-NP

Dynamic light scattering (DLS). For particle size and polydispersity index (PDI) measurement, the stock solution of **J-NS** or **J-NP** was diluted with deionized water and passed through a 0.45 μm filter. Measurements were made in triplicate at 25 °C using Zetasizer NanoZS. Zetasizer Nano software (version 7.12) was used to analyze the data.

Transmission electron microscopy (TEM). Typically, 5 μL of diluted aqueous solution of **J-NS** or **J-NP** was dropped to a 200-mesh carbon coated copper grid and air-dried for 3 days. TEM observations were conducted on a Talos F200C electron microscope at an acceleration voltage of 200 kV.

Atomic force microscopy (AFM). Typically, AFM images were acquired with a Nanoscope V system operating in peakforce tapping mode under ambient condition. SNL-A cantilevers with a resonance frequency of ca. 65 kHz were used. The samples were prepared by dip coating about 50 μL of diluted aqueous solution of **J-NS** or **J-NP** onto freshly cleaved mica surfaces.

Scanning electron microscopy (SEM). The SEM samples were prepared according to the procedure for preparing the TEM sample. The copper grids were investigated using a MERLIN Compact (ZEISS) operating at 5 kV to obtain SEM images.

Stability studies of J-NP. Several **J-NP** solutions were prepared as follows. UV-vis absorption spectra of the obtained **J-NP** solutions were recorded daily over a period of 7 days.

*(i) Stability of **J-NP** upon diluting*. Five diluted solutions of **J-NP** were obtained through diluting with PBS starting from a solution of **J-NP** (10 μM **BDP**) at 25 °C.

(ii) Stability of **J-NP** *in saline.* Saline solution was added to the stock solution of **J-NP** to produce a saline solution of **J-NP** (10 μM **BDP**; 9.0% w/v NaCl) at 25 °C.

(iii) Stability of **J-NP** *in cell culture medium.* The stock solution of **J-NP** was added to a cell culture medium (DME/F12 supplemented with 10% heat-inactivated FBS, 100 U/mL penicillin, and 100 μg/mL streptomycin) at 25 °C to give a final solution of **J-NP** suspended in cell culture medium (10 μM **BDP**).

Calculation of fluorescence quantum yield. The fluorescence quantum yield of **BDP** was calculated according to the following equation:

$$\Phi_{fl,sample} = \Phi_{fl,st} \frac{F_{sample} A_{st}}{F_{st} A_{sample}} \frac{{\eta_{sample}}^2}{{\eta_{st}}^2} \quad \ldots(1)$$

where F_{sample} and F_{st} are the measured area of fluorescence emission peak by the sample and standard, respectively. A_{sample} and A_{st} are the absorbance at the excitation position by the sample and standard, respectively. η are the refractive index of the solvent. Cresyl violet (CV) in methanol was used as the standard sample [F_{st} = 0.54].[4,5] Measurements were carried out in 1 cm quartz cuvettes with a total sample volume of 3 mL.

Detection of singlet oxygen ($^1O_2$) generation using DPBF or QDPBF as probe.[2] For **BDP**, DPBF was added to a DMSO solution of **BDP** to give a final DMSO solution of **BDP** (1.0 μM). The solution was then subjected to 655 nm laser irradiation (0.1 W/cm^2) for 70 s. For **BDP** J-aggregate, DPBF was added to the solution of **BDP** J-aggregates in DMSO/water mixture (60/40 v/v) to give a final solution of **BDP** J-aggregates (1.0 μM **BDP**). The solution was then subjected to 808 nm laser irradiation (1.0 W/cm^2) for 70 s. For **J-NP**, QDPBF was added to an aqueous solution of **J-NP** to give a final aqueous solution of **J-NP** (2.0 μM **BDP**). The solution was then subjected to 785 nm laser irradiation (2.5 mW/cm^2) for 70 s. The UV-vis absorption spectra were recorded at 10 s intervals to evaluate the photosensitivity in producing $^1O_2$.

Evaluation of photobleaching resistance. The aqueous solution of **J-NP** (10 μM **BDP**) was irradiated under a 785 nm laser (0.5 or 2.0 W/cm^2) for 10 min to reach a plateau of temperature elevation, followed by naturally cooling down to the ambient temperature. The temperatures were recorded during five circles of heating and cooling progresses by a FLIR E60 camera. UV-vis absorption spectroscopy was also adopted to evaluate the photothermal stability of the **J-NP**. An aqueous solution of ICG was used as a control.

Calculation of the photothermal conversion efficiency. The photothermal conversion efficiencies were calculated as the methods reported in the literature.[6] Typically, 1.0 mL of **J-NP** aqueous solution (10 μM **BDP**) was irradiated with a 785 nm laser continually, until the temperature elevation reached a steady state, and then naturally cooling down to the ambient temperature. The temperature was measured every 30 s with an IR thermal imaging camera (E60, FLIR). The water was used as a control. The photothermal conversion efficiency (PCE) was calculated according to the following Equation (2):

$$\text{PCE} = \frac{hA(T_{max} - T_{surr}) - Q_{dis}}{I(1 - 10^{-A785})} \quad \ldots\ldots\ldots\ldots(2)$$

where h is the heat transfer coefficient, A is the superficial area of the container, T_{Max} and T_{Surr} are the

maximum temperature reached and ambient temperature, respectively, Q_{Dis} represents heat dissipated from the laser mediated by the solvent and container. The value of hA is derived from Equation (3):

$$\mathrm{hA} = \frac{m_D c_D}{\tau} \quad \ldots\ldots\ldots\ldots\ldots\ldots\ldots\ldots (3)$$

where m_D and c_D are the mass and heat capacity of water, τ is the time constant for heat transfer of the system determined by the Equation (4):

$$\tau = -\frac{t}{ln^{\theta}} \quad \ldots\ldots\ldots\ldots\ldots\ldots\ldots\ldots (4)$$

where t is time and θ is the dimensionless driving force of the temperature fall period. The value of θ is derived from Equation (5):

$$\theta = \frac{T_{surr} - T}{T_{surr} - T_{max}} \quad \ldots\ldots\ldots\ldots\ldots\ldots\ldots (5)$$

Q_{dis} is the heat dissipation from the light absorbed by the solvent and is calculated according to the Equation (6):

$$Q_{dis} = \frac{m_D c_D (T_{max,water} - T_{surr})}{\tau_{water}} \quad \ldots\ldots (6)$$

where τ_{water} and $T_{max,water}$ are determined to be 235.5 and 27.9 ˚C, respectively.

Cellular uptake in vivo. Balb/c mice bearing 4T1 xenografts were randomly divided into two groups (n = 4): (i) **J-NS** and (ii) **J-NP** (50 μL, 0.9 mg/kg), when tumor volumes reached about 150 mm^3. After 0.5 h of *i.t.* administration with **J-NS** or **J-NP**, tumors were retrieved and washed with PBS. The tumor tissues were enzymolyzed into suspensory cells. The collected cells were lysed through repeated freezing and thawing in water, followed by centrifuged (12000 rpm, 30 min). The residue was then dissolved in THF to obtain a **BDP** solution for quantification by UV-vis spectroscopy. Cellular uptake of **J-NS** or **J-NP** was calculated by the standard curve of **BDP**.

Antitumor PTT performance of J-NS in vivo. 4T1 cells (~1 × 10^6) suspended in 100 μL of PBS were subcutaneously injected into the right flank of each mouse. When 4T1 tumor volumes reached about 130 mm^3, Balb/c mice bearing 4T1 xenografts were randomly divided into three groups (n = 4): (i) PBS (50 μL), (ii) **J-NS** (50 μL, 0.9 mg/kg), and (iii) **J-NS** + laser irradiation (785 nm, 0.5 W/cm^2, 10 min). The tumor sizes and body weights were recorded every other day.

4. Supplementary Figures

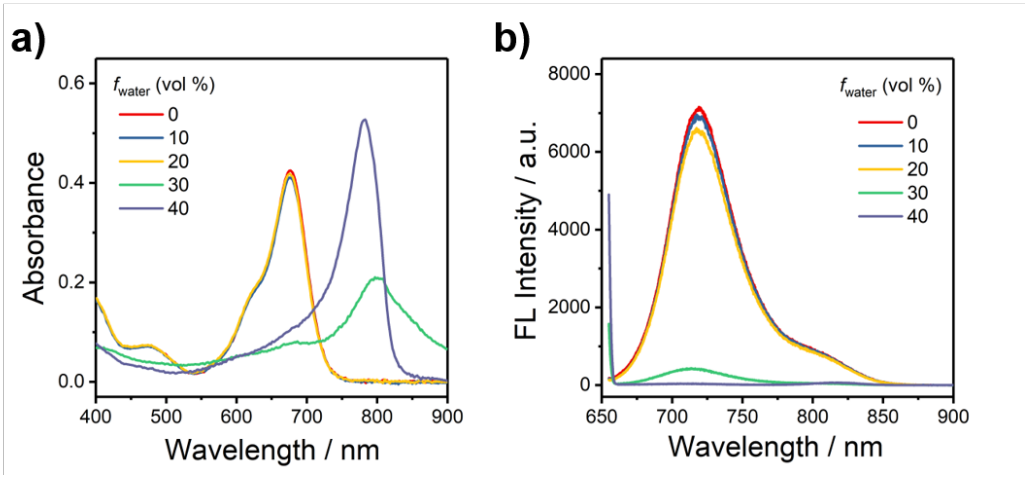

Figure S1. UV-vis absorption (a) and fluorescence emission (b) spectra (λ_{ex} = 650 nm) of **BDP** (5.0 μM) in DMSO/water mixture with various water fractions (f_{water}) from 0 to 40% (vol %).

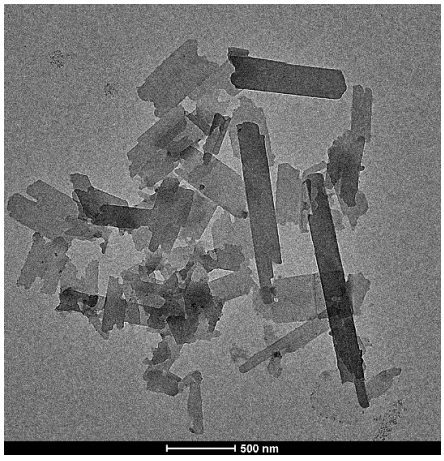

Figure S2. Typical transmission electron microscopy (TEM) image of **BDP** J-aggregate in the DMSO/water (60/40 v/v) mixture.

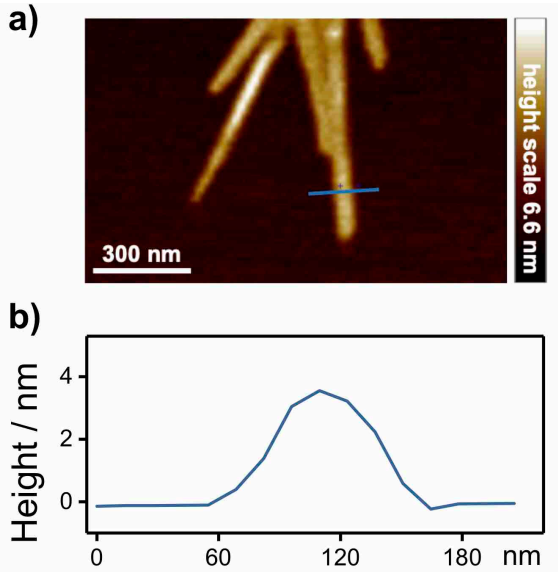

Figure S3. Typical AFM height image (a) of **BDP** J-aggregate with cross-sectional profile (b) along the blue line.

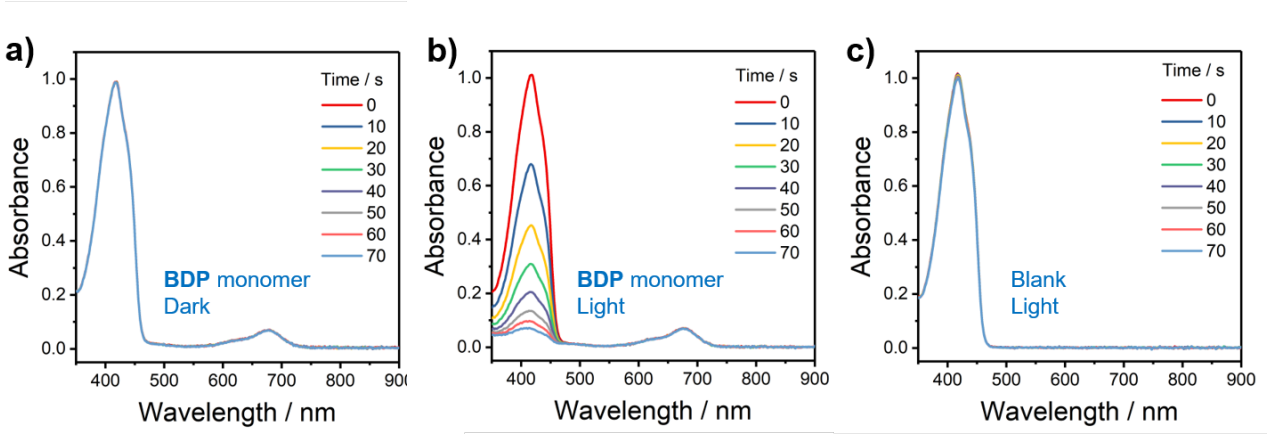

Figure S4. (a,b) Time-dependent UV-vis absorption spectra of DPBF within DMSO solution of 1.0 μM **BDP** in dark (a) or upon light irradiation (b). (c) Time-dependent UV-vis absorption spectra of DPBF only upon light irradiation. The light source is a 655 nm laser.

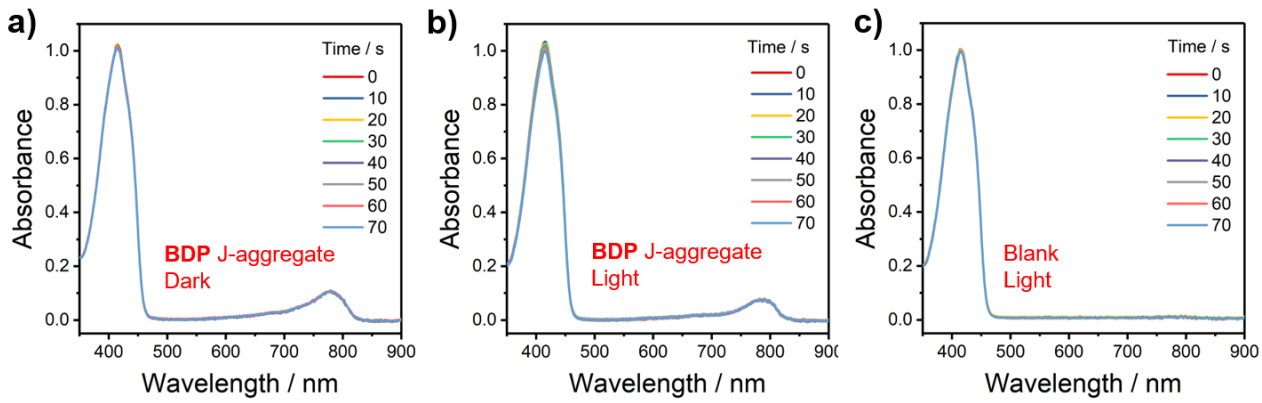

Figure S5. (a,b) Time-dependent UV-vis absorption spectra of DPBF within the solution of **BDP** J-aggregate (1.0 μM **BDP**) in DMSO/water mixture in dark (a) or upon light irradiation (b). (c) Time-dependent UV-vis absorption spectra of DPBF only upon light irradiation. The light source is an 808 nm laser.

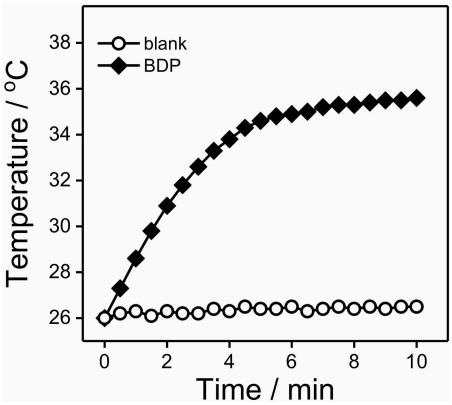

Figure S6. Evaluation of the photothermal capability of **BDP** in DMSO *via* recording the solution temperature upon laser irradiation (655 nm, 0.3 W/cm^2).

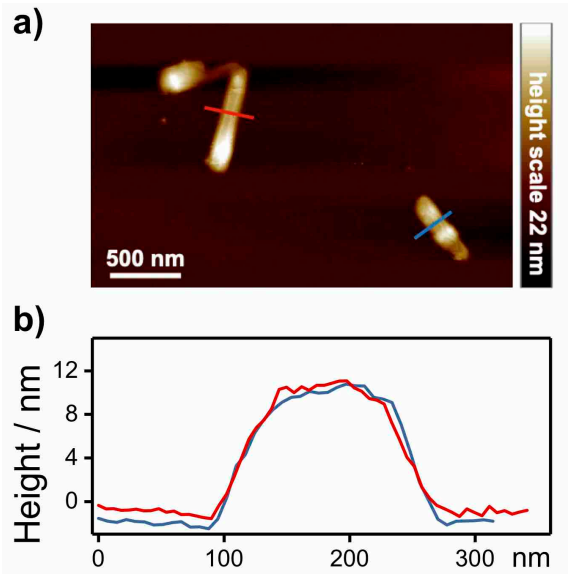

Figure S7. Typical AFM height image (a) of **J-NS** with cross-sectional profiles (b) along the red and blue lines.

Figure S8. Optical photograph recorded for the aqueous solution of **BDP** nano-assemblies in the absence (left) or presence (right) of PEG-PCL.

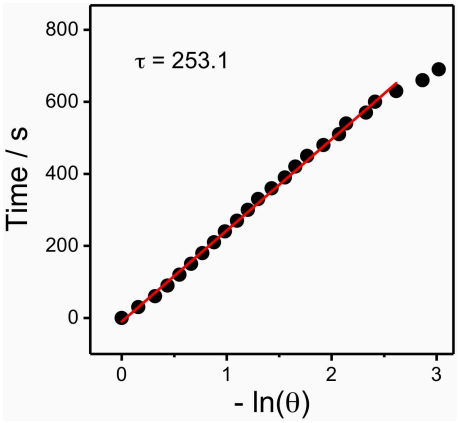

Figure S9. Time *versus* the negative natural logarithm of the temperature in the cooling process for **J-NS**. The fitted value was used to calculate the PCE of **J-NS**. Concentration 10 μM **BDP**.

Figure S10. Optical photograph of the lyophilized powder of the filtrate after ultrafiltration.

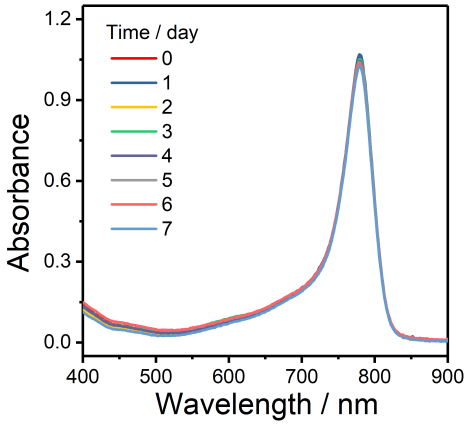

Figure S11. UV-visible absorption spectra recorded for freshly prepared and aged **J-NP** in PBS (1×, pH 7.4).

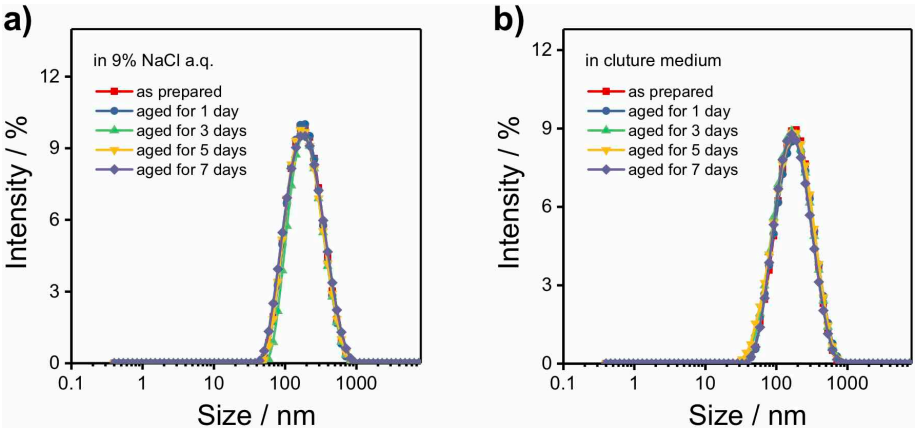

Figure S12. Size distribution recorded for **J-NP** in (a) saline solution (9.0% NaCl w/v) or (b) serum-containing cell culture medium (10% FBS) at different time intervals.

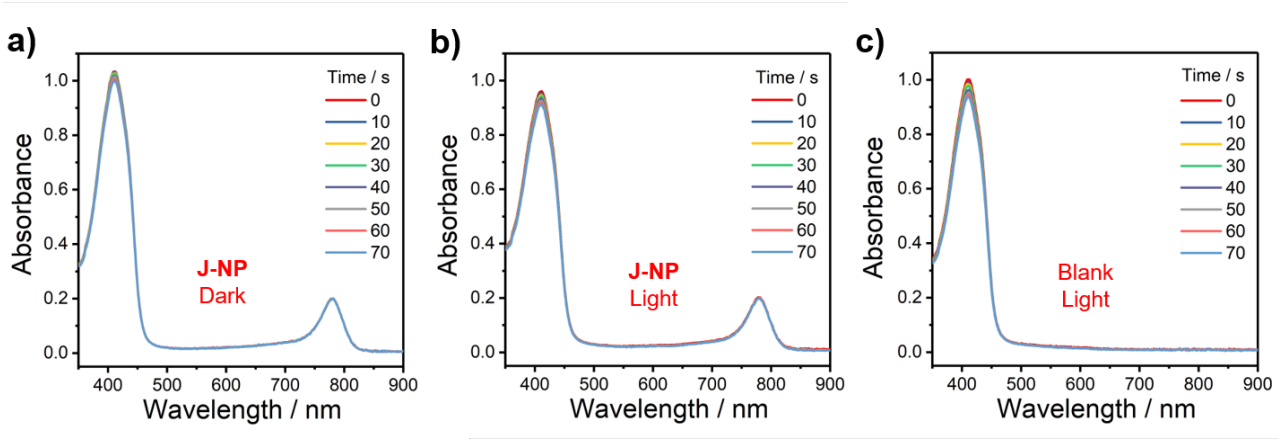

Figure S13. (a,b) Time-dependent UV-vis absorption spectra of QDPBF within aqueous solution of **J-NP** (2.0 μM **BDP**) in dark (a) or upon light irradiation (b). (c) Time-dependent UV-vis absorption spectra of QDPBF only upon light irradiation. The light source is a 785 nm laser.

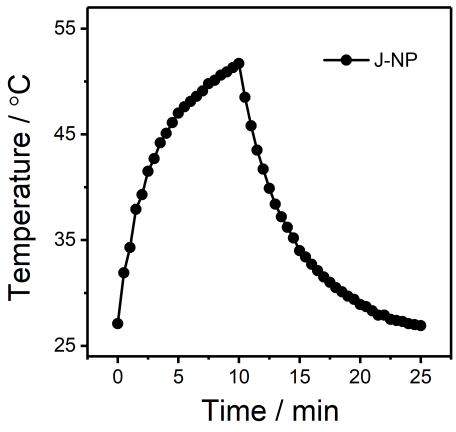

Figure S14. Temperatures of aqueous **J-NP** solution (10 μM **BDP**) as a function of laser irradiation time (785 nm, 0.5 W/cm^2).

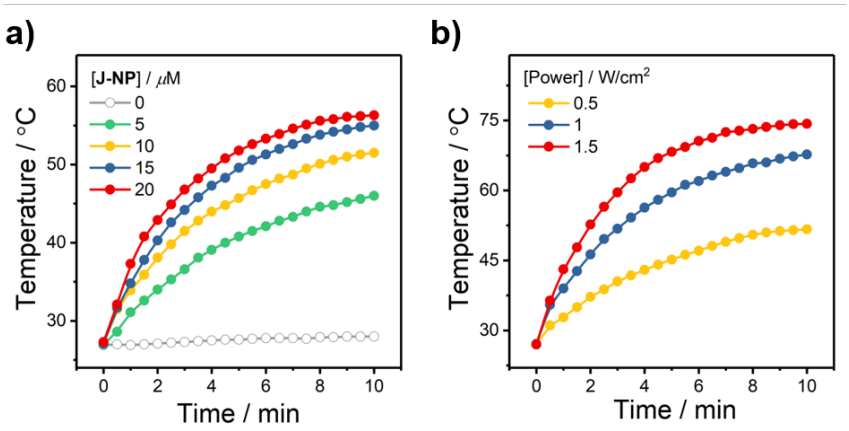

Figure S15. (a) Temperature elevations recorded for **J-NP** at different concentrations of **BDP** upon 785 nm laser irradiation (0.5 W/cm^2). (b) Time-dependent temperature changes recorded for **J-NP** (10 μM **BDP**) upon 785 nm laser irradiation with varying laser intensities as indicated. The results represent the average of three independent experiments.

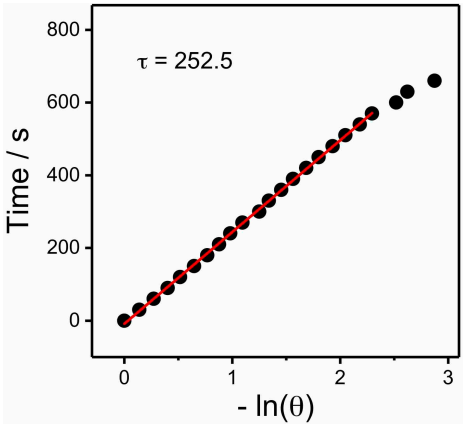

Figure S16. Time *versus* the negative natural logarithm of the temperature in the cooling process for **J-NP**. The fitted value was used to calculate the PCE of **J-NP**. Concentration 10 μM **BDP**.

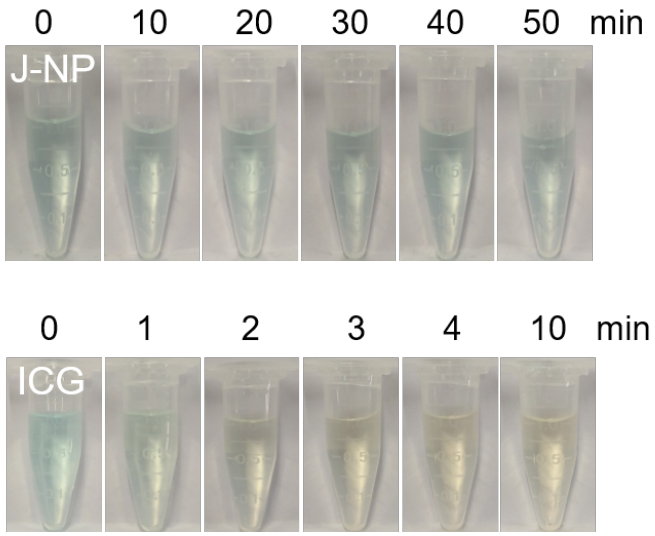

Figure S17. Optical photographs of aqueous solutions of **J-NP** (top line) and ICG (bottom line) in PBS after 785 nm laser irradiation (0.5 W/cm^2) for different time.

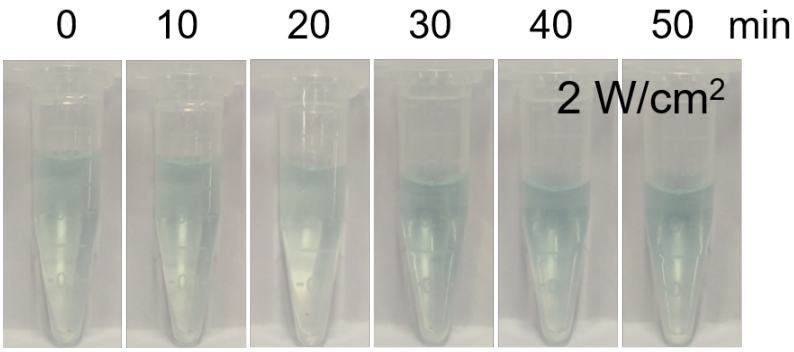

Figure S18. Optical photographs of aqueous solution of **J-NP** in PBS after 785 nm laser irradiation (2.0 W/cm^2) for different time.

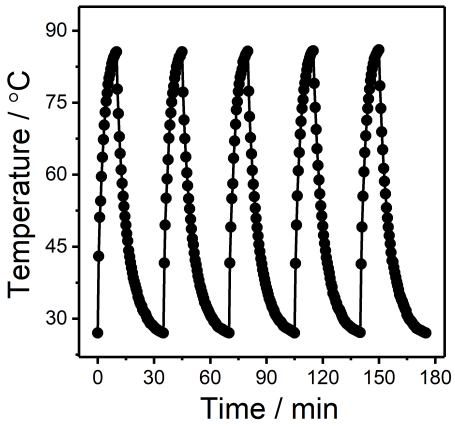

Figure S19. Temperature changes recorded for aqueous solution of **J-NP** (10 μM **BDP**) during 5 cycles of 785 nm laser irradiation (2.0 W/cm^2; 10 minutes per cycle).

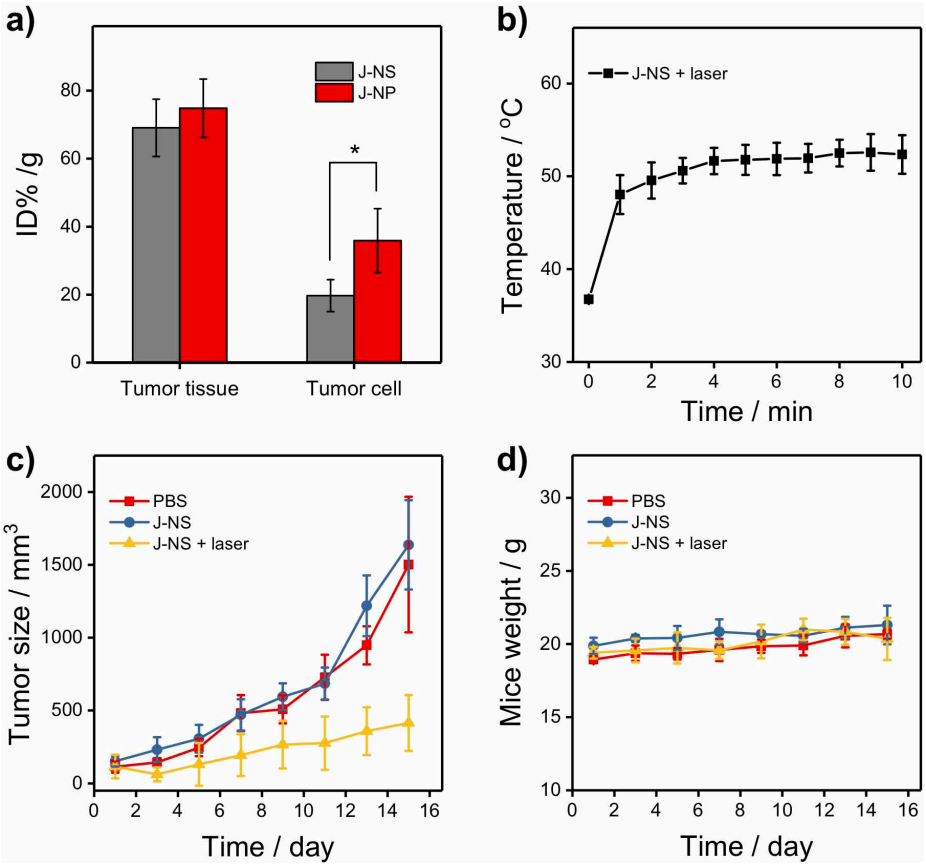

Figure S20. (a) Comparison of the *in vivo* cellular uptake ability of **J-NS** and **J-NP** in 4T1 tumors. (b) Mean temperatures in the tumor sites recorded for 4T1 tumor-bearing mice treated with **J-NS** under 785 nm laser (0.5 W/cm^2) irradiation for different time intervals. Data is mean ± SD (n = 4). (c) Tumor sizes and (d) body weights of mice in different treatment groups as indicated. Data is mean ± SD (n = 4).

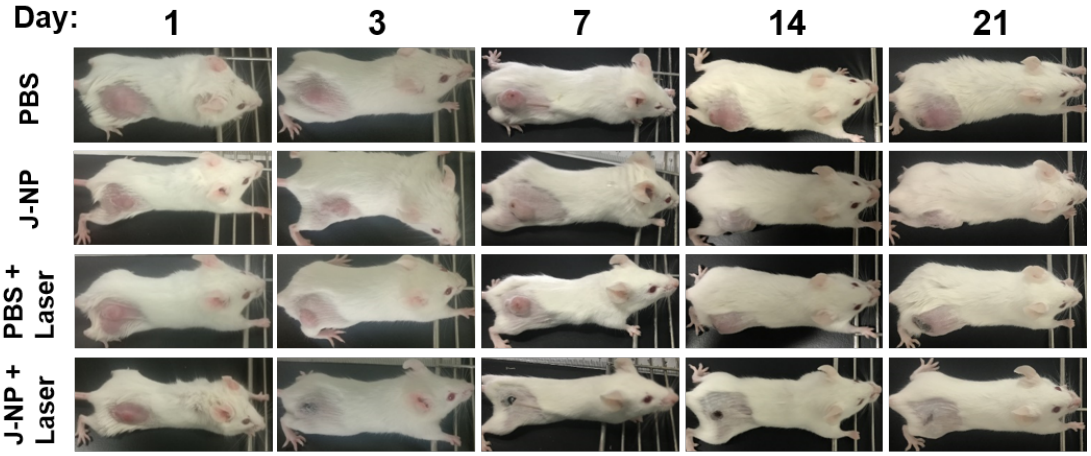

Figure S21. Typical optical photographs of tumor-bearing mice in different treatment groups during three weeks of observation.

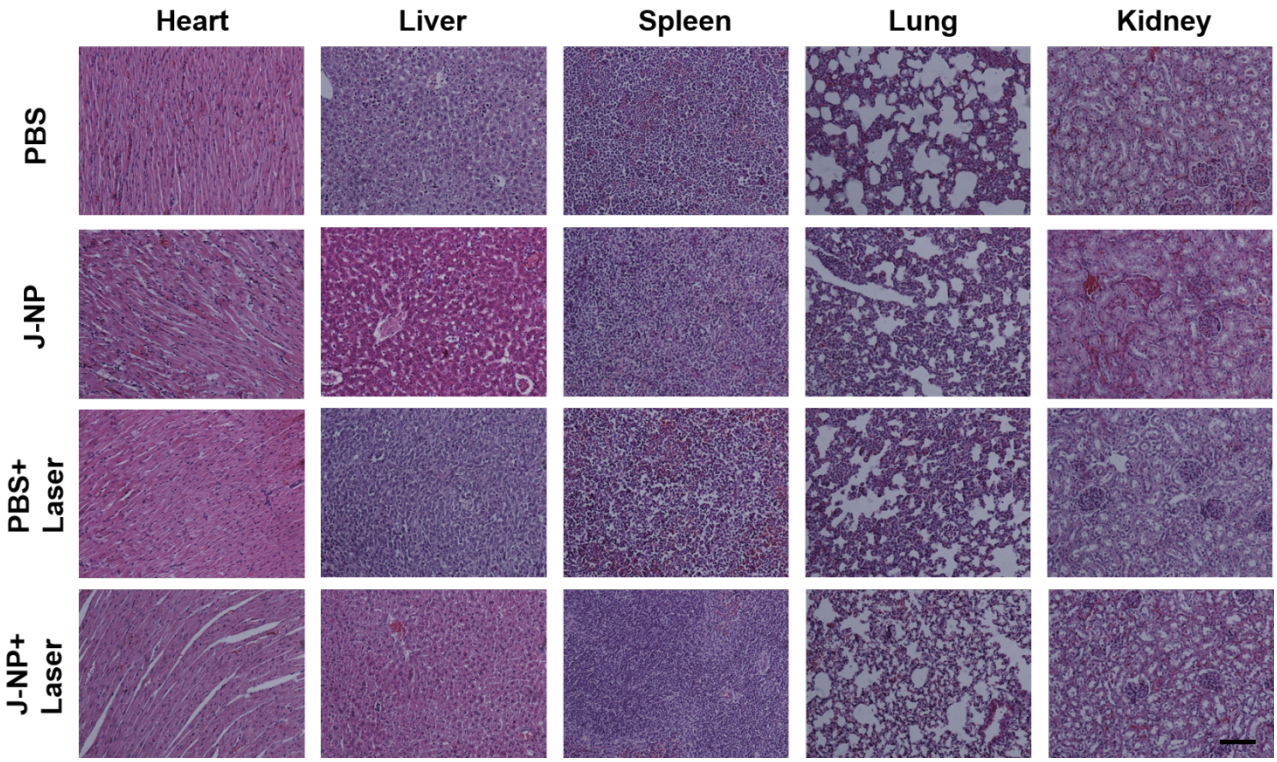

Figure S22. (a) H&E costaining images of major organs (heart, liver, spleen, lung, and kidney). Tissues were dissected from each group after three weeks of observation. Scale bar: 100 μm.

5. ^{1}H NMR spectra

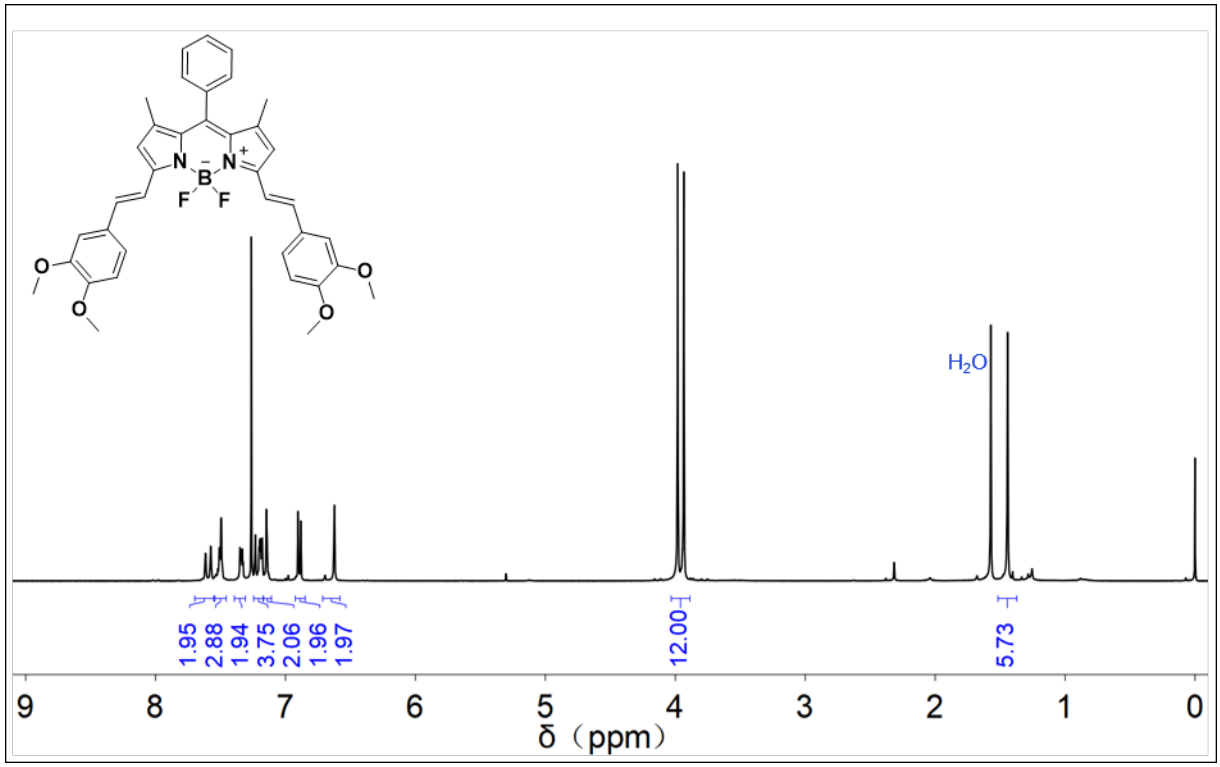

Figure S23. ^{1}H NMR spectrum (400 MHz) of **BDP-H** in $CDCl_3$ at 25 °C.

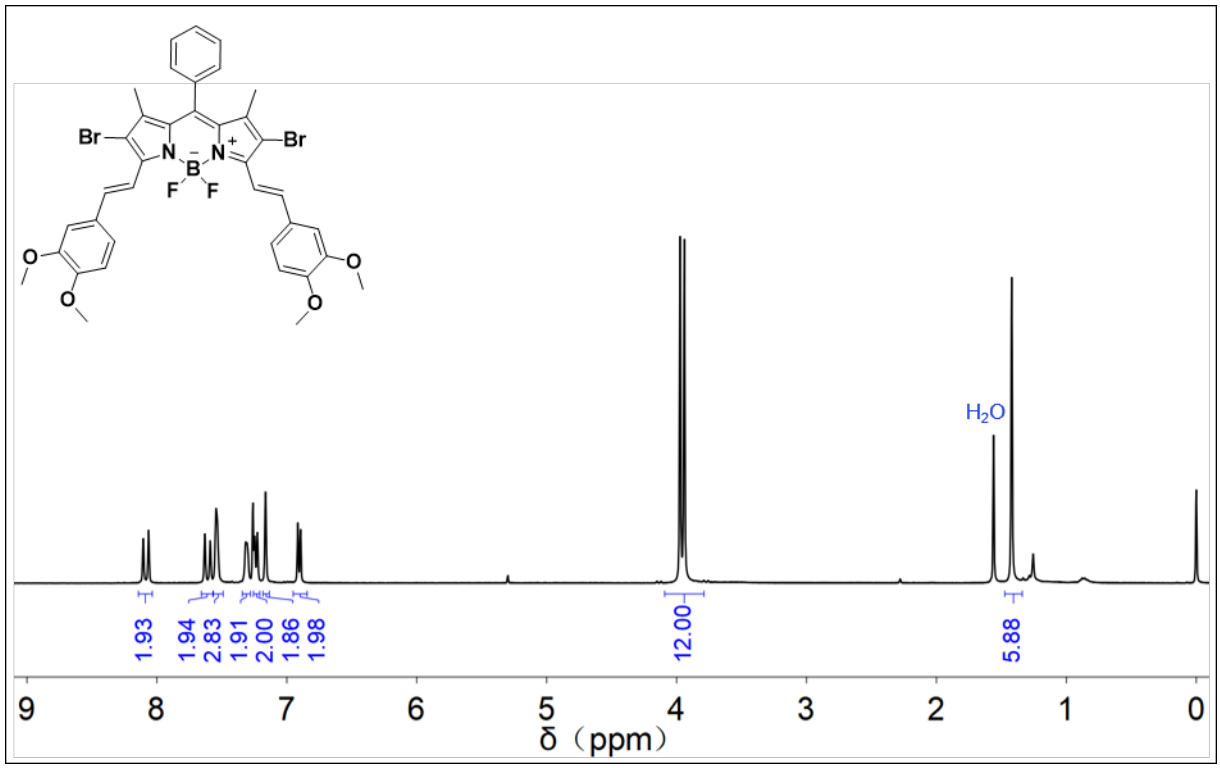

Figure S24. ^{1}H NMR spectrum (400 MHz) of **BDP** in $CDCl_3$ at 25 °C.

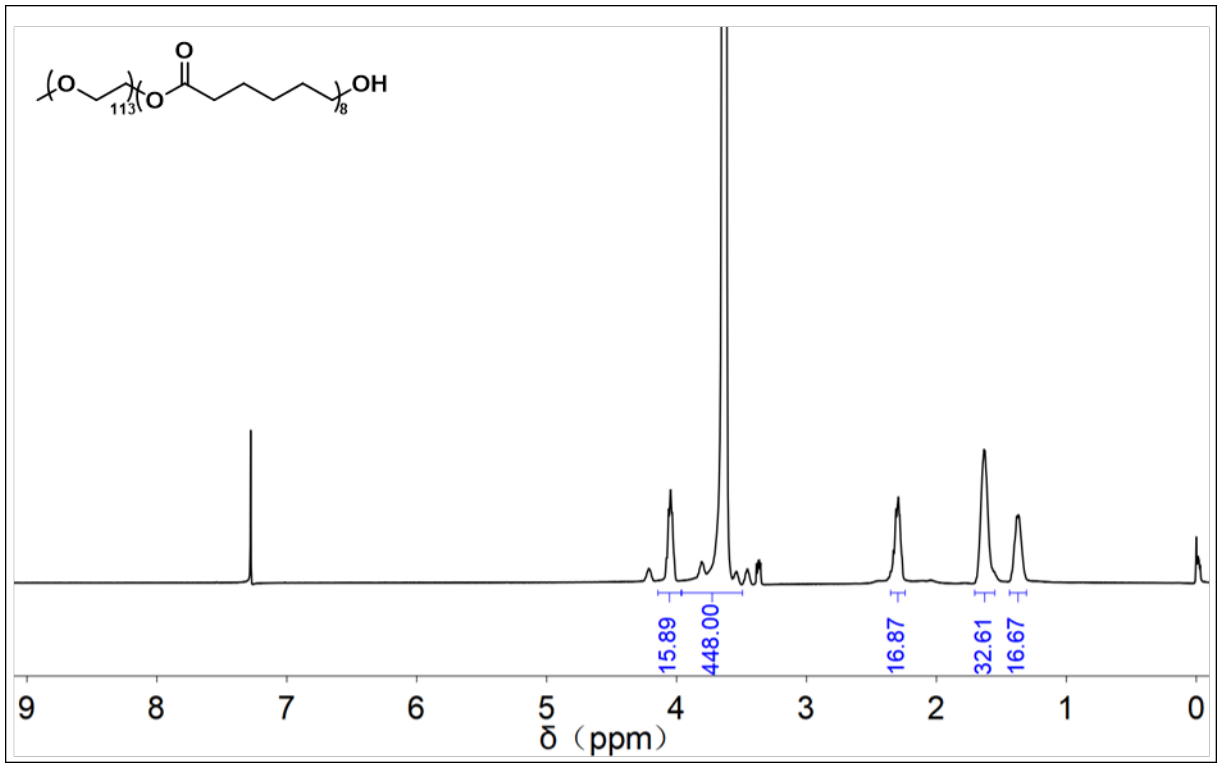

Figure S25. ^{1}H NMR spectrum (400 MHz) of **PEG-PCL** in $CDCl_3$ at 25 °C.

6. References

(1) Wang, Y.; Tang, L.; Sun, T.; Li, C.; Xiong, M.; Wang, J. Self-Assembled Micelles of Biodegradable Triblock Copolymers Based on Poly(ethyl ethylene phosphate) and Poly(ε-caprolactone) as Drug Carriers. *Biomacromolecules* **2008**, *9*, 388.

(2) Amat-Guerri, F.; Lempe, E.; Lissi, E. A.; Rodriguez, F. J.; Trull, F. R. Water-Soluble 1,3-Diphenylisobenzofuran Derivatives Synthesis and Evaluation as Singlet Molecular Oxygen Acceptors for Biological Systems. *J. Photoch. Photobio.* **1996**, *A 93*, 49-56.

(3) Su, M.; Yan, X.; Guo, X.; Li, Q.; Zhang, Y.; Li, C. Two Orthogonal Halogen-Bonding Interactions Directed 2D Crystalline Supramolecular J-Dimer Lamellae. *Chem. Eur. J.* **2020**, *26*, 4505-4509.

(4) Zhang, X.; Yang, X. Singlet Oxygen Generation and Triplet Excited-State Spectra of Brominated BODIPY. *J. Phys. Chem. B* **2013**, *117*, 5533−5539.

(5) Magde, D.; Brannon, J. H.; Cramers, T. L.; Olmsted, J. Absolute Luminescence Yield of Cresyl Violet. A Standard for the Red. *J. Phys. Chem.* **1979**, *83*, 696-699.

(6) Keith Roper, D.; Ahn, W.; Hoepfner, M. Microscale Heat Transfer Transduced by Surface Plasmon Resonant Gold Nanoparticles. *J. Phys. Chem. C* **2007**, *111*, 3636-3641.